293SF Metabolic Flux Analysis during Cell Growth and Infection with an Adenoviral Vector

I. Nadeau,[†,‡] D. Jacob,[†] M. Perrier,[‡] and A. Kamen*[,†]

Institut de recherche en biotechnologie, CNRC, 6100 avenue Royalmount, Montréal, Québec H4P 2R2, Canada, and École polytechnique de Montréal, Campus de l'Université de Montréal, Montréal, Québec, Canada

Metabolic flux quantification of cell culture is becoming a crucial means to improve cell growth as well as protein and vector productions. The technique allows rapid determination of cell culture status, thus providing a tool for further feeding improvements. Herein, we report on key results of a metabolic investigation using 293 cells adapted to suspension and serum-free medium (293SF) during growth and infection with an adenoviral vector encoding the green fluorescence protein (GFP). The model developed contains 35 fluxes, which include the main fluxes of glycolysis, glutaminolysis, and amino acids pathways. It requires specific consumption and production rate measurements of amino acids, glucose, lactate, NH_3, and O_2, as well as DNA and total proteins biosynthesis rate measurements. Also, it was found that extracellular protein concentration measurement is important for flux calculation accuracy. With this model, we are able to describe the 293SF cell metabolism, grown under different culture conditions in a 3-L controlled bioreactor for batch and fed-batch with low glucose. The metabolism is also investigated during infection under two different feeding strategies: a fed-batch starting at the end of the growth phase and extending during infection without medium change and a fed-batch after infection following medium renewal. Differences in metabolism are observed between growth and infection, as well as between the different feeding strategies, thus providing a better understanding of the general metabolism.

Introduction

Recombinant adenovirus is now an established tool for gene delivery and a promising viral vector for gene therapy (Kay and Woo, 1994; Trapnell, 1993; Trapnell and Gorziglia, 1994). The 293-Human Embryo Kidney cells, preferably adapted to suspension, are the complementary cells mainly used for the production of recombinant adenoviruses. However, three major limitations are still to be overcome before the technology is fully established. These limitations are safety, immunogenicity, and eventual gene packaging capacity (Briand and Kahn, 1993). This is addressed by the re-engineering of adenovirus vectors as well as associated complementary cell lines. Originally, the recombinant adenoviruses are engineered as defective vectors, since they cannot replicate in normal cells but only in 293 cells containing the E1 replicative-essential region of adenovirus. These recombinant adenoviruses are used in 18% of the gene therapy clinical trials, which implicate mainly the CFTR gene transfer (cystic fibrosis transmembrane conductance regulator) (Boucher and Knowles, 1994; Crystal et al., 1994) but also the TK gene (thymidine kynase) and the p53 gene, both for the treatment of certain cancers. It may also be used for other monogenic or chronic diseases.

To produce clinical grade viral vector stocks, large volume and high-density cell cultures are required. The freshly produced adenoviral vector must be purified from residual cell debris, serum proteins, etc. before application in clinical trials. To facilitate the purification process, serum-free medium is now increasingly used. Therefore, a 293 cell line was adapted to grow in serum-free medium (293SF) (Côté et al., 1998). However, to improve the production of adenoviruses with this cell line and medium, a robust process must be developed to operate high-density suspension cultures of 293 cells. A fed-batch process is the rational way for proceeding toward this objective. Previous studies with 293S cells in suspension, in conventional medium with 5% serum, have demonstrated that addition of glucose and amino acids permitted infection at a cell density of 3×10^6 cells/mL without compromising the specific production of the recombinant protein expressed (Garnier et al., 1994; Nadeau et al., 1996). The titers reached are in the range of 2000 pfu/mL. Also it was proven that a low-glucose fed-batch culture contributes to limitation of lactate accumulation in the cultures and associated toxic effects on cell growth and adenovirus expression.

Metabolic flux analysis is a powerful tool that permits the evaluation of biochemical rates inside the cell on the basis of simple measurements and mass-balancing techniques. It is increasingly used to evaluate cultures and optimize processes. In this report we used a metabolic model of 35 fluxes, dedicated to study the 293 cell metabolism during growth and infection by an adenovirus vector, which include the catabolism pathways of glucose, glutamine, and 17 amino acids.

This work was initiated to study the 293SF cell metabolism in the same conditions as the original cell line with serum supplementation. It was first shown that the titers in SFM were lower than those obtained in the

* Ph: (514) 496-2264. Fax: (514) 496-6785. E-mail: Amine.kamen@nrc.ca.

10.1021/bp000098l CCC: $19.00 Published 2000 by the American Chemical Society and American Institute of Chemical Engineers
Published on Web 09/19/2000

original process, reaching levels of 500 pfu/mL. This metabolic flux study evaluates the effect of different culture conditions on the cell's central metabolism and identifies metabolic patterns during growth and infection. The analysis will also permit identification of the pathways which are used to fulfill the energy requirement of the cell, in order to design in the future the best feeding strategy for these cells. To our knowledge, this is the first metabolic flux analysis with the 293 cells during growth and infection.

Materials and Methods

Cells, Medium, and Virus. The 293SF cells were derived from human kidney fibroblasts transformed with Ad5 DNA and express the E1A and E1B proteins constitutively (Graham et al., 1977). The 293SF cells were obtained by adapting 293S cells in serum-free medium (Côté et al., 1998). The 293SF cells were maintained in a 50 mL shake flask at 37 °C, 7% CO_2, by diluting twice weekly to cell densities of $1-2 \times 10^5$ cells/mL with the medium described herein. After 3 months of subculturing, the cells are discarded and a new aliquot is thawed.

Low-calcium serum-free medium (LC-SFM) was prepared from H-SFM (Gibco, Grand Island, NY). The medium was completed with 0.1% (v/v) lipids (Gibco), 0.1% (v/v) BSA (Intergen Company, Purchase, NY), and 0.1% (v/v) Pluronic F-68 (Gibco, Grand Island, NY). For the low-glucose fed-batch, the process is described elsewhere (Siegwart et al., 1999). For the fed-batches, a mixture of glutamine 400 mM (Sigma, St. Louis, MO), glucose 300 g/L (Sigma), and MEM Amino acids (Gibco) is used.

The adenovirus used for infection was an adenovirus type 5 containing the green fluorescence protein (GFP), under the control of the CMV promoter (Ad5 GFPq). The viral stock titer was 7.5×10^{12} pfu/mL.

Bioreactor. The cultures were done in a Chemap CF2000 (Mannedorf, Switzerland) 3.5-L bioreactor and 20-L bioreactor for the low-glucose fed-batch. The 20-L culture conditions with low-glucose fed-batch are described elsewhere (Siegwart et al., 1999). For the 3.5 L culture, the vessel was equipped with four surface baffles and two marine impellers. The temperature was maintained at 37 °C with a water jacket. Dissolved oxygen and pH probes were mounted for monitoring and control purposes. The pH was controlled at 7.1 by intermittent addition of 1 M NaOH. DO was not controlled at the beginning of cell growth, and the vessel was supplied with air having 10% CO_2. As soon as it dropped to 30% air saturation, it was controlled at this level. The control was operated with a PI and mass flow controller programmed on FIX MMI software (Intellution, Norwood MA). On-line data acquisition was also performed with the same software.

Cell Culture Conditions and Infection. Cells were inoculated at around 0.3×10^6 cells/mL from two 500-mL shake flasks in which the cell density was around 1×10^6 cells/mL. The cells were centrifuged and resuspended in fresh LC-SFM before inoculation of the bioreactor. Samples were taken every 6−9 h. The cells were infected when the cell density reached 1×10^6 cells/mL (Batches 1 and 2).

For the batch infection (Inf B) experiment, the cells were harvested and centrifuged to replace the medium with fresh LC-SFM. The virus was added at the same time. At 24 h after infection a mixture of 1× MEM amino acid, 4 mM glutamine, and 25 mM glucose was supplemented.

For the fed-batch infection (Inf FB) experiment, the virus was added to the culture in 100 mL fresh LC-SFM medium. Fed-batch was started right after with a flow rate of 0.01 mL/min, increasing to a final flow rate of 0.06 mL/min. This feeding was based on previous experiments. The mixture was composed of 150 mL MEM amino acids, 25 mL glucose 300 g/L, and 50 mL glutamine 400 mM.

Analytical Method. Viable and total cells were counted using a hemacytometer (Hausser Scientific, Horshaw, PA). Viability was assessed by dye exclusion method using erythrosine B. For DNA analysis, the procedure was as follows. First a sodium citrate buffer was prepared (SSC 20×) with 175.3 g/L NaCl and 88.2 g/L trisodium citrate. The pH was adjusted to 7.0. Approximately 1×10^6 cells were disrupted in SSC 1×/0.4% v/v SDS (Sodium dodecyl sulfate) for 10 min at 37 °C. Thereafter, 5 mL SSC 1× was added. The samples were also sonicated lightly. Next, 10 μL of the samples were then distributed in triplicate in a 96 well plate and 90 μL of SSC 1× was added, as well as 100 μL of 1 mg/mL Hoescht 33258. The plate was read in a fluorometer (Bio-Tek Instruments, Winooski, VT) at absorbing and emitting wavelengths of 360 and 460 nm, respectively. The standard curve was made from a stock solution of herring sperm DNA at 1 mg/mL (Sigma) and diluted in SSC 1× ranging from 50 to 3.12 μg/mL; 10 μL of one sample was added to the standards to mimic the sample conditions. For the dry weight estimation, approximately 1×10^8 cells were pelleted in a preweighed tube of 1.5 mL. The pellet was dried in an oven at 60 °C for about 48 h or until the weight remained constant (Xie and Wang, 1994). Total protein and extracellular proteins were assayed using the Dc Protein Assay (Bio-Rad, Hercules, CA). Prior to the analysis the 1×10^6 cells pellet was disrupted using the buffer consisting of 0.5% Triton X-100, 1 mM EDTA, and 0.2 mM phenylmethylsulfonylfluoride (PMSF) (Xie and Wang, 1994). For analysis of amino acids in the supernatant, a HPLC column was used as described elsewhere (Kamen et al., 1991). For determination of cells' amino acid content, a 1×10^6 cells pellet, washed twice with PBS, was hydrolyzed in a 2 M HCl solution for 24 h at 100 °C. The pellet was then neutralized and filtered prior to HPLC analysis. The Biolyzer (Kodak, New Haven, CT) was used for the analysis of glucose, lactate, and ammonia. The virus titer was assayed as follows: 1×10^6 293S cells were distributed in a 6-well plate, with 1 mL fresh DMEM without calcium, 5% BCS (Hyclone, Logan, UT). The virus was released with three freeze−thaw cycle and diluted in fresh medium, and 25 μL of the dilutions was added to the wells. Incubation was held 20 h with agitation. The cell pellet was fixed with 500 μL of PBS and 500 μL of 4% formaldehyde at 4 °C for 30 min. Percentage of fluorescent cells was done with flow cytometry (FACS). One fluorescent cell corresponds to one infectious particle (IVP) when less than 30% cells were fluorescent.

Metabolic Model. The metabolic model used in this study involves 35 fluxes. The model is derived from a previous version detailed in Nadeau et al. (2000). Glycolysis, glutaminolysis, amino acid degradation, TCA cycle, and protein production and internalization are considered.

As previously mentioned, some fluxes were set to zero. Many authors (Bonarius et al., 1996) have reported that the glutamate dehydrogenase activity is very low in animal cells. Cysteine contributes mainly to the formation of glutathione and therefore is not included in the model (Bannai, 1986; Bannai and Ishii, 1988). Tryp-

tophan is an intermediate to NAD+ and NADP+ component and therefore is also not included (Brown, 1996). Threonine can undergo several pathways, but as suggested by Salway (1994), the degradation to pyruvate may be the main pathway. We also did not consider the pentose-phosphate cycle in our analysis, assuming that all the ribose-5-phosphate (Rib5P) goes for the formation of nucleotides. Also the three main anaplerotic reactions were pooled in one reaction. We also considered that the cell tends to maintain a constant pool of NADH and NADPH as well as other intracellular nutrients. This assumption is called pseudo steady state (Bonarius et al., 1996; Bonarius et al., 1997; Schmidt et al., 1998) and will be discussed later.

In this model, a flux for the protein internalization was added. Cells proceed to pinocytosis and endocytosis, to directly incorporate extracellular medium and some macromolecules. In our serum-free medium the main source of protein is bovine albumin serum (BSA) at 1 g/L, followed by transferrin (0.01 g/L) and insulin (0.01 g/L). Therefore, we can consider BSA as the only source of protein, and as was reported by Kooistra and Lloyd, (1986) albumin can be internalized quite rapidly. Also Kooistra and Lloyd (1985) reported that albumin is degraded predominantly inside lysosomes in the cell. Some authors (Nyberg et al., 1999) have already considered the internalization of small peptides in their flux calculation, and they have reported better modeling over results obtained neglecting protein internalization.

Also we adapted the metabolic model to infection. It is important to consider the DNA replication due to an adenoviral infection. It was already demonstrated that cellular DNA is completely inhibited after infection (Pina and Green, 1969). Hodge and Scharff (1969) have demonstrated that the cellular DNA synthesis shut-off starts after 9 h of infection, no matter in which phase the cells are upon infection. Cells in G1 phase will stop to grow and therefore will not double, but cells in S phase will stop only in G1 phase and therefore cells will double once again. Thus it is not surprising to see 50−75% of cell growth after infection. At 24 h after infection, 10^6 new viral genomes are formed per cell (Green, 1967; Green, 1970; Pina and Green, 1969). After infection, no new cellular messenger RNA (mRNA) is formed, and it is reported that at the last phase of infection up to 95% is viral mRNA (Lindberg et al., 1972). Thus RNA measurement is less important since messenger RNA quantity remains unchanged in steady state (Babich et al., 1983; Philipson et al., 1975). It is also reported that the host protein synthesis is inhibited early after infection and relayed by the viral protein synthesis (White et al., 1969).

From this information, the cells dry weight, as well as its protein and DNA content appears important to be measured. It is assumed that RNA synthesis remains unchanged. Also we have measured amino acids composition of the protein, as described, to identify potential variation between growth and infection.

Rate and Flux Calculation. The consumption and production rates of the following metabolites were used in the model for flux calculation: glucose, lactate, ammonia, O_2, CO_2, all of the amino acids except for tryptophan, cysteine and cystine, total intracellular and extracellular protein, and finally DNA. The consumption and production rates were calculated as follows. Samples were taken every 6−9 h except for O_2 and CO_2, which were monitored on-line. Intermediate points were interpolated every hour using polynomials. Then the slope was evaluated in order to estimate the rates.

We then have a 35 × 35 matrix of stoichiometric coefficients with a rank of 35 and a condition number of 147. Usually a condition number around 100 is recommended for flux calculations. We added an extra steady-state hypothesis on NADH and NADPH, thus providing a matrix of size 36 × 35, with a rank of 35, while this new measurement does not permit an extra flux calculation. Also the condition number reduces to 94, which is now acceptable.

If we apply a mass balance around the biomass, we have

$$\frac{dS}{dt} = KF - DS - Q + P \tag{1}$$

where S is the internal cellular concentration of metabolites, K the 36 × 35 matrix of stoichiometric coefficients, F the vector of 35 fluxes, DS represents the dilution due to volume variation of the cells, and $-Q + P$ represents the vector of the specific consumption and production rate of metabolites. We assume that the cell volume does not change and that the internal metabolite concentration does not vary over a short period of time. This assumption is referred to as pseudo-steady-state assumption (PSS assumption). These assumptions are used for flux calculations by many authors (Bonarius et al., 1997; Pissarra and Henriksen, 1998; Savinell and Palsson, 1992; Takiguchi et al., 1997). This simplifies the equation to an algebraic system of linear equation:

$$KF = Q - P \tag{2}$$

and F can be resolved:

$$F = \text{pseudoinverse}(K) \cdot (Q - P) \tag{3}$$

The fluxes shown were divided in four main groups, i.e., (i) the main fluxes of glycolysis, (ii) the main fluxes of glutaminolysis, (iii) amino acid fluxes, and (iv) the Krebs cycle fluxes. The glycolysis fluxes are composed of F1, glucose to pyruvate; F2, pyruvate to lactate; F3, pyruvate to Krebs cycle. The glutaminolysis fluxes are $F5_{tot}$, the net flux of glutamate to α-ketoglutarate, which comprises all transamination reactions; $F8_{tot}$, the net flux of glutamine to glutamate, which also includes the transamination process of aspartate to asparagine; and finally F4, the production of alanine. The amino acid fluxes represent the fluxes of different essential amino acids to the Krebs cycle or the glutamate pool. The Krebs cycle fluxes are also shown: F30 and F31 are the fluxes from acetyl-CoA to α-ketoglutarate and the fluxes F32, F33, F34, and F35 are the fluxes on the left side of the cycle. F10 represents the anaplerotic pathways in which components such as malate and oxaloacetate are recycled in the glycolysis pathway as pyruvate or oxaloacetate. See Figure 1 and Table 1 for more details on the biochemical reactions.

pCO_2 Measurement. pCO_2 measurements were used to verify if the model was predictive. We could compare the pCO_2 calculated with the model to the pCO_2 measured in the culture. If we apply a CO_2 mass balance in the liquid phase, we have

$$V_L \frac{dC_{CO_2}}{dt} = k_L{}^{CO_2} a(C^*_{CO_2} - C_{CO_2})V_L + X_v\, p_{CO_2} V_L - k_1 C_{CO_2} + k_{-1} C_{HCO_3} C_{H^+} \tag{4}$$

where V_L is the liquid volume, C the concentration, $k_L{}^{CO_2}a$ the CO_2 liquid transfer rate, and k_1 and k_{-1} are the direct

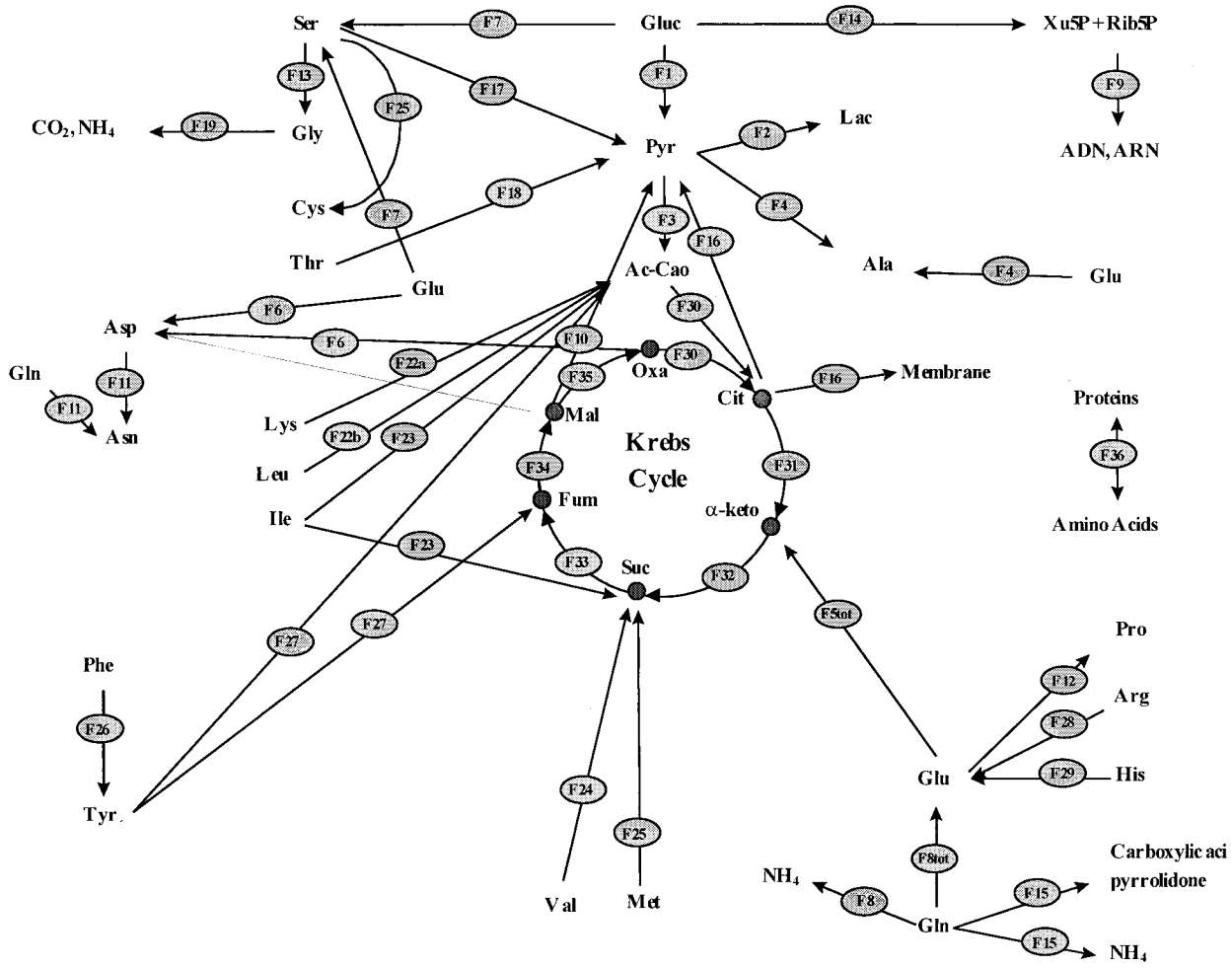

Figure 1. Metabolic network. α-Keto, α-ketoglutarate; Ac-CoA, acetyl-CoA; AcOle, oleic acid; Arg, arginine; Asn, asparagine; Asp, aspartate; Cit, citrate; Cte, cysteine; Fum, fumarate; Gluc, glucose; Gln, glutamine; Glu, glutamate; Gly, glycine; His, histidine; Ile, isoleucine; Lac, lactate; Leu, leucine; Lys, lysine; Mal, malate; Met, methionine; Oxa, oxaloacetate; Phe, phenylalanine; Pro, proline; Pyr, pyruvate; Rib5P, ribose-5-P; Ser, serine; SucCoA, succinyl-CoA; Thr, threonine; Tyr, tyrosine; Val, valine; Xu5P, xilulose-5-P.

and reverse rate constant for H_2CO_3 dissociation. At the operating pH (around 7.0), H_2CO_3 is solely in a dehydrated form: $H_2O + CO_2$. Furthermore HCO_3^- is not decomposed to H^+ and CO_3^-. Therefore, this equilibrium reaction is not considered in the evaluation of CER. Concerning the equilibrium reaction between HCO_3^- and H_2CO_3 (present in the form of CO_2), we consider that when a small pH variation occurs in the medium, the equilibrium is rapidly attained. These assumptions lead to the following equality:

$$k_1 C_{CO_2} = k_{-1} C_{HCO_3} C_{H^+} \tag{5}$$

If we apply a CO_2 mass balance in the gas phase, we have

$$\frac{P V_g}{RT}\frac{dx_{CO_2}}{dt} = (x^E_{CO_2} - x_{CO_2})F_g - k_L^{CO_2} a (C^*_{CO_2} - C_{CO_2})V_L \tag{6}$$

where P is the pressure, V_g is the gas volume in the headspace, R is the gas constant, T is the temperature, $x^E_{CO_2}$ and x_{CO_2} are the CO_2 gas molar fraction at the entrance and exit, respectively, and F_g is the gas flow rate. Combining the two mass balances, we have

$$V_L\frac{dC_{CO_2}}{dt} = X_v q_{CO_2} V_L + \left((x^E_{CO_2} - x_{CO_2})F_g - V_g\frac{dx_{CO_2}}{dt}\right)\frac{P}{RT}$$

but

$$V_g\frac{dx_{CO_2}}{dt} \cong 0$$

and

$$V_L\frac{dC_{CO_2}}{dt} \ll X_v q_{CO_2} V_L$$

and

$$\left((x^E_{CO_2} - x_{CO_2})F_g - V_g\frac{dx_{CO_2}}{dt}\right)\frac{P}{RT} \tag{7}$$

The last assumption will be verified in a desorption analysis, to verify if the CO_2 concentration varies in the medium. If there are no cells in the medium, the preceding equation simplifies to

$$V_L\frac{dC_{CO_2}}{dt} = \left((x^E_{CO_2} - x_{CO_2})F_g - V_g\frac{dx_{CO_2}}{dt}\right)\frac{P}{RT}$$

but

$$V_g\frac{dx_{CO_2}}{dt} = 0 \tag{8}$$

Table 1. Biochemical Reactions

F_1	GLUC ⇔ 2PYR + 2ATP + 2NADH
F_2	PYR + NADH + H^+ ⇔ LAC
F_3	PYR + CoA → ACCoA + NADH + CO_2 + H^+
F_4	PYR + GLU ⇔ ALA + α-KETO
F_5	GLU ⇔ α-KETO + NADH + NH_4
F_6	OXA + GLU ⇔ ASP + α-KETO
F_7	GAP + GLU → SER + α-KETO + NADH
F_8	GLN + H_2O → GLU + NH_4^+
F_9	2GLN + $^5/_4$ASP + RIB5P + $^1/_2$GLY + $6^6/_8$ATP + $^5/_8$NADPH → ADN/ARN + $^3/_4$NADH + $^3/_4$FUM + 2GLU
F_{10a}	MAL → PYR + CO_2 + NADPH + H^+
F_{10c}	PYR + ATP + CO_2 → OXA + H^+
F_{11}	ASP + GLN + ATP ⇔ ASN + GLU
F12	GLU + ATP + 2NADPH + $2H^+$ → PRO
F13	SER ⇔ GLY
F14a	GLC6P + ATP → Rib5P + 2NADPH + H^+ + CO_2
F15	GLN → Carboxylic Acid Pyrolidone + NH_4
F16	2(9CIT + 17ATP + 9CoA + 16NADPH) → AcOLE + 18OXA
F17	SER → PYR + NH_3
F18	THR → CO_2 + 2NADH + $2H^+$ + $FADH_2$ + NH_4 + PYR
F19	GLY ⇔ CO_2 + NH_4 + NADH + H^+
F20	CTE + O_2 + α-KETO → PYR + GLU
F22a	LYS + 2α-KETO + NADPH → 2ACCoA + $2CO_2$ + 4NADH + $3H^+$ + $FADH_2$ + 2GLU
F22b	LEU + α-KETO + ATP → 3 ACCoA + GLU + CO_2 + NADH + H^+ + $FADH_2$
F23	ILE + α-KETO + ATP → SUCCoA + ACCoA + CO_2 + 2NADH + $2H^+$ + $FADH_2$ + GLU
F24	VAL + α-KETO + ATP → SUCCoA + 3NADH + H^+ + $FADH_2$ + $2CO_2$ + GLU
F25	MET + SER + 2ATP → CTE + SUCCoA + NADH + H^+ + CO_2 + NH_3
F26	PHE + O_2 + NADPH + H^+ → TYR
F27	TYR + α-KETO + $2O_2$ → FUM + 2ACCoA + GLU
F28	ARG + α-KETO → 2GLU + NADH + H^+ + urea
F29	HIS → GLU + NH_3
F30	OXA + ACCoA → CIT
F31	CIT → α-KETO + CO_2 + NADPH + H^+
F32	α-KETO → SUCCoA + NADH + H^+ + CO_2
F33	SUCCoA → FUM + ATP + $FADH_2$
F34	FUM ⇔ MAL
F35	MAL ⇔ OXA + NADH + H^+

and therefore, it is possible to study the CO_2 desorption in different cases of incoming CO_2. Here we studied the desorption in water with 2.45 g/L of $NaHCO_3$ and an adjusted pH of 6.88 in order to mimic the conditions of LC-SFM. The incoming air was at 300 mL/min, with 2% O_2 and %CO_2 varying from 0 to 10%. The pH remained constant during the experiment, and therefore it is valid to neglect the equilibrium reactions. If the desorption term is negligible, a good approximation is then

$$X_v q_{CO_2} V_L = -((x^E_{CO_2} - x_{CO_2}) F_g) \frac{P}{RT} \tag{9}$$

Some authors (Gray et al., 1996; Nyberg et al., 1999) used this approximation, but they had a term of incoming and outgoing medium because they were in perfusion. Here, no fresh medium was added; instead fed-batches were operated and nutrients were added at low rates.

Sensitivity Analysis. Sensitivity analysis is used to investigate which are the measurements that require a good precision. We simulated a 10% variation on each measurement, we calculated the fluxes as indicated by eq 3 and sorted the mean relative error overall the fluxes, for every time point. Then the maximum relative error was sorted overall the time points and compiled in the Results section.

Intracellular Concentration. The intracellular concentration was also investigated in order to verify the validity of the pseudo-steady-state assumption. The samples were prepared as follows: 1×10^7 cells were pooled in 1.5 mL vials and centrifuged at 14 000 rpm for 1 min. The pellet was then rinsed twice with cold PBS and frozen immediately on dry ice. If not used immediately, it was frozen at −80 °C. For glucose, lactate, and ammonia analysis, the samples were thawed on ice and 0.4 mL of perchloric acid at 1 M was added. Tubes were immediately vortexed and allowed to stand 5 min. Then, 0.125 mL of K_2CO_3 2 M was added and a precipitate appeared. Next, 0.05 mL of triethanolamine 0.5 M/EDTA 5 mM pH 7.6 was added to neutralize the pH. The sample was then filtered on a 0.2 μm membrane, and the supernatant was ready to use.

For amino acid analysis, we added 0.5−1 mL of 0.5 M perchloric acid, and the cell pellet was then vortexed and allowed to stand for 5 min on ice before it was sent for amino acid analysis.

The internal variation rate was then calculated and converted to an external variation, i.e., the variation was considered on the external volume basis as follows:

$$r = \frac{s_2 - s_1}{t_2 - t_1} \cdot \frac{V_{int}}{V_{ext}} \tag{10}$$

The cell volume was taken as 17.7×10^{-10} mL as reported by Schmid and Keller (1992).

Results

Sensitivity Analysis. Table 2 presents the sensitivity analysis that was performed on the model with the data of Batch 1 and Inf B. Measurements that are very sensitive are glucose, lactate, glutamine, asparagine, DNA, extracellular proteins, lysine, ammonia, and oxygen. Measurements that do not lead to significant errors are glycine, aspartate, glutamate, and methionine. For the other measurements, the errors are case-dependent. All the methods presented good reproducibilities and were done with standard curves. The only measurement that may present an error higher than 10% is the cells' total protein content, which was done with a standard curve using albumin. Since the albumin and cell composition in amino acids are not identical, we can misestimate the total protein content. Fortunately, this measurement is not the most sensitive.

Pseudo-Steady-State Assumption. Most of the previous analyses (Bonarius et al., 1997; Pissarra and Henriksen, 1998; Savinell and Palsson, 1992; Takiguchi et al., 1997) were done in chemostat in order to maintain homeostasis in the cells. However, in this study, the experiments were done in the same conditions as in the process, which consists of a fed-batch followed by a lytic infection. Therefore, the PSS assumption had to be verified. In Table 3, we report the variation in the concentration that occurred over 72 h in cells. The first column gives the results obtained by Schmid and Keller (1992). Columns 2 and 3 give the actual concentrations that were measured at the beginning of growth and after 72 h. The fourth column gives the variation over time. The fifth column gives the variation reported to the external volume. The sixth column is reported on the number of cells and is to be compared to the actual specific rate of consumption and production of the last column.

We see in Table 3 that the internal concentration variation is at least 100 times lower than the actual specific rate of consumption and production in the medium, it represents in the worst case 1% of the

Table 2. Maximum Mean Relative Error over Time on Metabolic Flux When a 10% Variation Is Processed on a Measure

variation on	growth (Batch 1)	infection (Inf B)
glucose	1995.94	714.71
lactate	1880.57	660.53
serine	36.68	10.68
glycine	4.79	4.92
alanine	32.29	11.11
aspartate	1.65	3.48
asparagine	150.14	64.39
glutamine	270.31	107.72
glutamate	7.92	2.82
membrane	62.45	7.43
ADN/ARN	186.80	43.35
proteins	76.11	87.57
extracellular proteins	181.50	118.04
threonine	8.21	21.64
phenylalaline	26.05	34.27
tyrosine	23.07	5.59
valine	39.33	5.31
methionine	6.11	8.04
arginine	50.91	26.72
histidine	23.49	7.74
lysine	123.58	15.16
leucine	81.44	20.28
isoleucine	23.14	7.25
NH_3	122.58	127.25
O_2	479.90	216.34

external rate. Therefore, from these observations we can conclude that the pseudo-steady-state assumption is valid.

Cell Composition. In Table 4 are compiled results on the cell composition for cell growth. We report data on total protein, DNA, and RNA as well as dry weight. The values represent mean values over two to three samples taken during cell growth.

In general, the data seem consistent with what is reported in the literature (Xie and Wang, 1994). Total protein represents approximately 60% of dry weight for the 293 cell, but DNA varies from 1% to 5%. These values in pg/cell are used in the model.

Figure 2 presents the dry weight, total protein, and DNA content of the cells. We see that this content varies during infection. For Inf B the dry weight, amount of DNA, and total protein increased after infection reaching maximum values between 35 and 40 h. While the DNA content increased throughout infection and continues to increase after 35 h, in Inf FB the DNA content decreased after a certain time.

The next graph (Figure 3) shows the percentage of amino acids in total protein during growth and infection. The variations are not significant, and therefore we used a mean value over time to include in the matrix of stoichiometric coefficient. It was shown that these variations did not affect the flux calculation significantly (results not shown).

CO_2 Desorption. Table 5 shows the desorption of CO_2 as it was measured according to the procedure described in Materials and Methods.

From these results, we see that at higher CO_2 concentration, the desorption rate was also higher as the pH decreased. We also concluded that these values were 100 times lower (data not shown) than the CER, and therefore the CO_2 desorption due to HCO_3^- can be neglected for the calculation of pCO_2.

Figure 4 presents the calculated and measured pCO_2 for the model, which includes a balance on NADH and NADPH. We see clearly that in Figure 4 both series followed the same trend. Adding the NADH/NADPH balance to the model is more appropriate, as was also shown previously by other authors (Bonarius et al., 1996; Bonarius et al., 1997; Schmidt et al., 1998).

Cell Growth, Glucose and Glutamine Consumption, and Lactate and Ammonia Production. Prior to any metabolic flux calculation and in order to allow the reader to get a sense of the raw data obtained for the five experiments, consumption and production rates of the main metabolites are presented in Figure 5a−e.

In Figure 5a, the cell concentrations are shown for all the experiments. During the batch cultures, cells had similar growth curves. However, the cell concentrations at 60 h were, respectively, 1.7×10^6 and 1.2×10^6 cells/mL. Batch 2 reached a plateau phase much earlier than Batch 1, right after 40 h of growth. In the fed-batch with low glucose (fed-batch LG) the cells reached a plateau at around 45 h. The viability during growth phase was always above 90% in all cases (not shown). For the infection phase, we observed 50% growth for Inf B in the first 12 h, but for the Inf FB we observed up to 100% growth after 24 h. After the cell densities reached a maximum, the viable cell count decreased in both infections.

In Figure 5b, we see that the total glucose consumption for the fed-batch with low glucose concentration was also very low. The two batches followed the same glucose consumption. For Inf B with medium replacement the glucose consumption was slightly higher than Inf FB without medium replacement, 23 versus 20 mM. Figure 5c presents the total glutamine consumption. The fed-batch with low glucose and Batch 1 had the same glutamine consumption. Batch 2 had a slightly higher total glutamine consumption, 1.9 versus 1.2 mM for the other growth experiments. The glutamine consumption diminished at around 30 h. During infection, the glutamine consumptions were higher, 2.9 mM for Inf B and 8.2 mM for Inf FB. Figure 5d presents lactate production. As expected, the fed-batch with low glucose showed the lowest lactate production, 8.4 mM. The two batches followed the same trend, with 18 and 16 mM for Batch 1 and 2, respectively. The infection experiments both showed a higher lactate production, 48.5 mM for Inf B and 37.1 for Inf FB. It is noteworthy that Inf FB, which had no medium replacement, had a lower production even though it started with lactate at 15 mM. Finally, Figure 5e shows the ammonia production. The production of ammonia was not constant, and a lot of singularities were observed. Batch 1 experiment had a starting ammonia concentration of 0.7 mM, showing that glutamine was already degraded in the medium. However, no more ammonia was produced than in Batch 2 and fed-batch LG. The three runs produced approximately 1.5 mM. During Batch 1, the production was not very high at the beginning but increased between 20 and 30 h and decreased afterward. The infections showed a high ammonia level especially for the fed-batch, which produced approximately 3.5 mM compared to the batch that had produced 2.5 mM. An inflection point was also observed for Inf B at 20 h and at 28 h for Inf FB.

Virus Titer. We see in Figure 5f that in the two infection experiments the maximum titer was attained around 45 h after infection. During Inf B, up to 400 pfu/mL was measured, but for Inf FB, the virus titer was reduced to 75 pfu/mL, showing that this experiment did not produce as expected, suggesting that limiting nutrient conditions or inhibitory metabolite levels were reached.

Flux Calculation. To analyze the data further and to understand differences in metabolism, a flux analysis was completed integrating key nutrient measurements.

Table 3. Intracellular Concentration and Intracellular Nutrient Variation

	Schmid (1992) (1)	time 0 (2)	time 72 (3)	internal rate mM/h (4)	equiv extrnl rate mM/h (5)	equiv specific rate mmol/h × 10^9 cells (6)	specific rate consump (35 h) mmol/h × 10^9 cells (7)
lactate		51.91	51.91	0.00	0.00	0.00	5.79×10^{-1}
ammonia		4.90	4.96	-8.01×10^{-4}	-1.84×10^{-7}	-1.54×10^{-7}	4.51×10^{-4}
asp	2.98	3.91	1.68	3.10×10^{-2}	7.13×10^{-6}	5.48×10^{-6}	0.00
glu	10.91	14.49	6.57	1.10×10^{-1}	2.53×10^{-5}	1.95×10^{-5}	-5.67×10^{-3}
asn	1.22	0.65	0.34	4.38×10^{-3}	1.01×10^{-6}	7.76×10^{-7}	-6.14×10^{-3}
ser	1.92	1.78	0.54	1.72×10^{-2}	3.96×10^{-6}	3.05×10^{-6}	-1.07×10^{-2}
gln	2.67	4.04	1.74	3.20×10^{-2}	7.37×10^{-6}	5.67×10^{-6}	-3.61×10^{-2}
his	0.82	1.13	0.32	1.13×10^{-2}	2.60×10^{-6}	2.00×10^{-6}	-2.31×10^{-3}
pro	4.12	3.28	1.33	2.72×10^{-2}	6.25×10^{-6}	4.81×10^{-6}	N/D
thr	4.47	5.52	2.39	4.35×10^{-2}	1.00×10^{-5}	7.69×10^{-6}	-3.55×10^{-3}
arg	0.63	1.20	0.49	9.85×10^{-3}	2.27×10^{-6}	1.74×10^{-6}	-5.02×10^{-3}
ala	16.16	7.30	2.73	6.35×10^{-2}	1.46×10^{-5}	1.12×10^{-5}	1.04×10^{-2}
tyr	0.78	0.02	0.26	-3.33×10^{-3}	-7.66×10^{-7}	-5.89×10^{-7}	-3.31×10^{-3}
gly	8.24	12.62	3.64	1.25×10^{-1}	2.87×10^{-5}	2.21×10^{-5}	3.70×10^{-3}
met	0.11	0.02	0.13	-1.51×10^{-3}	-3.48×10^{-7}	-2.68×10^{-7}	-2.46×10^{-3}
val	0.75	1.63	0.64	1.38×10^{-2}	3.18×10^{-6}	2.45×10^{-6}	-7.54×10^{-3}
phe	0.55	0.26	0.26	-9.98×10^{-6}	-2.30×10^{-9}	-1.77×10^{-9}	-3.10×10^{-3}
ile	0.63	0.93	0.43	7.01×10^{-3}	1.61×10^{-6}	1.24×10^{-6}	-5.65×10^{-3}
leu	0.43	0.98	0.43	7.61×10^{-3}	1.75×10^{-6}	1.35×10^{-6}	-7.72×10^{-3}
lys	0.78	1.67	0.34	1.86×10^{-2}	4.27×10^{-6}	3.29×10^{-6}	-1.04×10^{-2}

Table 4. Cell Composition

	293 5-19S Nadeau (2000)		293SF/Batch 1		293SF/Batch 2		Xie (1994)	
	mean (pg/cell)	% w/w	mean (pg/cell)	% w/w	mean (pg/cell)	% w/w	mean (pg/cell)	% w/w
dry weight	279.00		288.00		302.50		250	
total proteins	178.83	64.10	161.00	55.90	179.70	59.40	183	73.2
total lipids	69.00	24.73					33.75	13.5
DNA	11.09	3.97	15.80	5.49	5.80	1.92	3.5	1.4
RNA							9.5	3.8

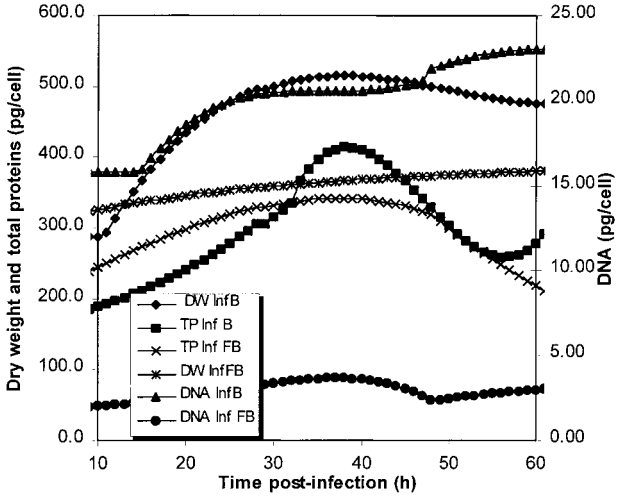

Figure 2. Dry weight (DW), total proteins (TP), and DNA content of 293SF cells during infection.

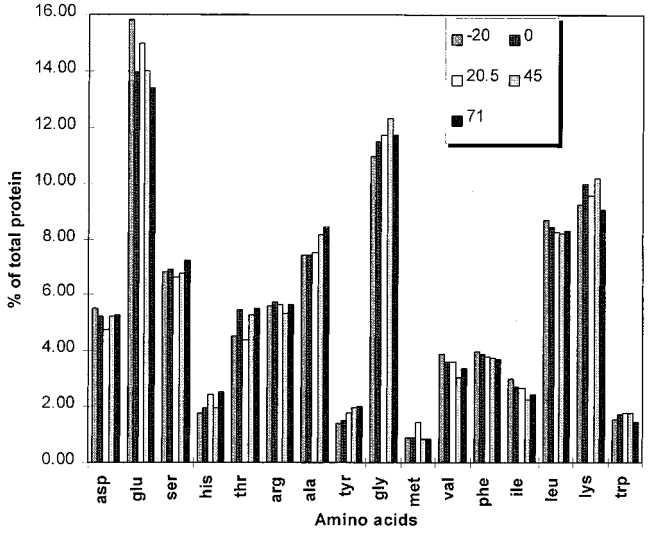

Figure 3. Amino acid composition of total proteins in 293SF cells during infection. Number in legend indicates postinfection time in hours.

Fluxes were segregated in four groups as explained in Materials and Methods. Flux computations were started at 20 h postinoculation for Batch 1, Batch 2, and Fed-Batch LG to avoid lag phases and transitory regimes and were started at 10 h postinfection for Inf B and Inf FB.

Figure 6 shows the main glycolytic fluxes, the flux from glucose to pyruvate (F1), the flux to lactate (F2), and the flux to acetyl-CoA (F3). The first two graphs (Figures 6a and 6b) show the glycolytic fluxes for both Batches 1 and 2. Noteworthy, the flux to acetyl-CoA (F3) is negative until 50 h of growth. For the fed-batch with low glucose (Figure 6c), the fluxes F1 and F3 were 3 times lower compared to the batches and F3 was always slightly negative.

Table 5. Rate of CO_2 Desorption

%CO_2	desorption (mol/min)	pH
0.61	-8.03×10^{-6}	7.83
0.85	-8.24×10^{-6}	7.83
5.02	-5.82×10^{-5}	7.28
5.02	-5.71×10^{-5}	7.29
10	-4.28×10^{-5}	7.00

For the two infections (Figure 7), the glucose fluxes were approximately constant. The lactate flux (F2) reached a peak at around 40 h for the batch (Inf B) and 50 h for the fed-batch (Inf FB). F2 in Inf FB was approximately half lower compared to Inf B. The glyco-

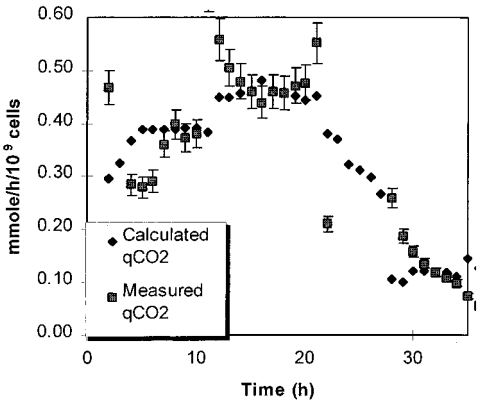

Figure 4. Calculated qCO_2 with the model versus measured qCO_2.

lytic fluxes (F1) are similar to those in the growth phase, while F3 was mostly positive during the two infection experiments.

Figure 8 shows the main glutaminolysis fluxes which comprise $F8_{tot}$, the sum of all the fluxes from glutamine to glutamate, $F5_{tot}$, the sum of all the fluxes from glutamate to α-ketoglutarate, and finally F4, the flux to alanine, one important product during cell cultures. The trends were very different from one experiment to the other. In Batch 1, the flux $F8_{tot}$ decreased rapidly at 29 h, becoming negative. For $F5_{tot}$ a maximum was observable for both batches, one at 22 h, the other at 29 h for Batch 1 and Batch 2, respectively. F4 was constant in the first batch but became negative at 50 h in the second batch. The fluxes $F8_{tot}$ and $F5_{tot}$ were 2−10 times lower for the fed-batch with low glucose (Figure 8c), while $F8_{tot}$ became negative at around 58 h.

For the infection phases (Figure 9), $F8_{tot}$ was mostly positive but two times higher in Inf FB. $F5_{tot}$ was mostly negative in both cases, but we observed a high peak between 28 and 34 h for Inf B. These fluxes were in the same order of magnitude as in the batch growth phase. F4 was mostly positive and low in all cases as in the growth phases.

Figure 10 shows the amino acids fluxes. During the late exponential phase both batch fluxes reached similar level (Figure 10A and B). For Batch 1, we observed a perturbation in the fluxes around 27 h, especially for phenylalanine (F26) and tyrosine (F27), which increased, and arginine (F28) and histidine (F29), which decreased. For Batch 2, we also observed a perturbation in the threonine flux (F18b) and histidine flux (F29) later on at 37 h, while some amino acids fluxes increased. For the low-glucose fed-batch, fluxes were approximately 2 times higher during growth but perturbations for most of the amino acids appeared between 50 and 60 h. The fluxes of lysine (F22a), leucine (F22b), isoleucine (F23), tyrosine (F27), and valine (F24) were the highest fluxes for the growth experiments.

In Figure 11, for Inf B a drastic increase at around 10 h after infection was observed, and these fluxes remained higher than in growth phase. Up to 80% of the amino acids fluxes were negative between 21 and 35 h after infection for both experiments. After 28 h most of the fluxes increased again, reaching values as high as 0.04 $mmol/10^9$ cells/h for Inf FB.

Figure 12 represents the Krebs cycle fluxes. During the exponential growth phase the fluxes were in the same order of magnitude for both batches, but F32, F33, and F34 decreased at the end of the growth phase for Batch 2. For both batches, F10 became negative at approximately 45 h. The fluxes were up to 2 times higher for the low-glucose fed-batch (Figure 12c) during the first 50 h of growth. Interestingly F10 was mostly positive at the beginning.

For the infection phase (Figure 13), the trends were also very different. For Inf B, we observed up to 2 times increase or decrease around 10 h and variations between 24 and 36 h after infection. The fluxes were approximately 2 times higher than in the growth phase. For Inf FB, some perturbations also occurred between 21 and 36 h. For both experiments, F10 is mostly negative.

Discussion

Batch Growth. The two batch growths were operated in the same conditions, and consequently they had the same growth profile. Consumption and production profiles of glucose and lactate were similar, and the main glycolytic fluxes were also similar for both batches. Interestingly F3 was negative during the exponential phase of both batches, showing that there must be an excess in acetyl-CoA and pyruvate might not have entered the Krebs cycle. Flux F3 is driven by the *pyruvate* dehydrogenase, and this enzyme was shown to be inactive in a lot of transformed cells. Therefore, it is not surprising to see low positive fluxes or even reversed fluxes (Mancuso et al., 1994; Petch and Butler, 1994).

The consumption and production of glutamine and ammonium were different in the two batches. In Batch 1, at around 15 h, ammonia production increased and consequently $F8_{tot}$ (net flux of glutamine to glutamate) dropped drastically at 29 h, even though glutamine was still at 2 mM and ammonium at 1.5 mM. We have shown previously that this ammonia concentration is not yet inhibitory to growth (Nadeau et al., 2000). It seemed that a high ammonia production initiated a metabolic shift toward less glutamine consumption. By this method, the cells might prevent the formation of more ammonia caused by glutamine consumption.

The source of glutamate had to be replenished by another pathway. Arginine and histidine were a good source of glutamate but produced ammonia too, so these fluxes (F28 and F29) decreased at 29 h, while phenylalanine and tyrosine degradation (F26 and F27) increased, thus producing glutamate without ammonia via transamination pathways. Therefore, we see a shift in the metabolism from arginine and histidine to phenylalanine and tyrosine in order to prevent ammonia accumulation while replenishing the glutamate pool. Interestingly, these changes did not seem to inhibit growth in any way.

In Batch 1, we see that the Krebs cycle fluxes reach steady-state rapidly; this can explain the constant growth rate for Batch 1. Batch 2 had Krebs cycle fluxes constant between 25 and 45 h, but some of the fluxes decreased afterward, resulting in an earlier plateau phase for these cells. $F5_{tot}$ was lower than $F8_{tot}$, showing that there is more glutamine consumption than glutamate consumption. Small perturbations were observed at 37 h. At that time, some amino acids fluxes increased, such as arginine (F28) and histidine (F29), thus replacing the glutamate source, but also threonine (F18b), lysine (F22a), and leucine (F22b), which feed the pyruvate and acetyl-CoA, pool. Then, the upper part of the Krebs cycle is fed and F35, F30, and F31 increased, but the Krebs cycle bottom part fluxes started decreasing at that time. This is mainly due to the fact that glutamine is fed less to the Krebs cycle and other amino acids metabolism such as phen-

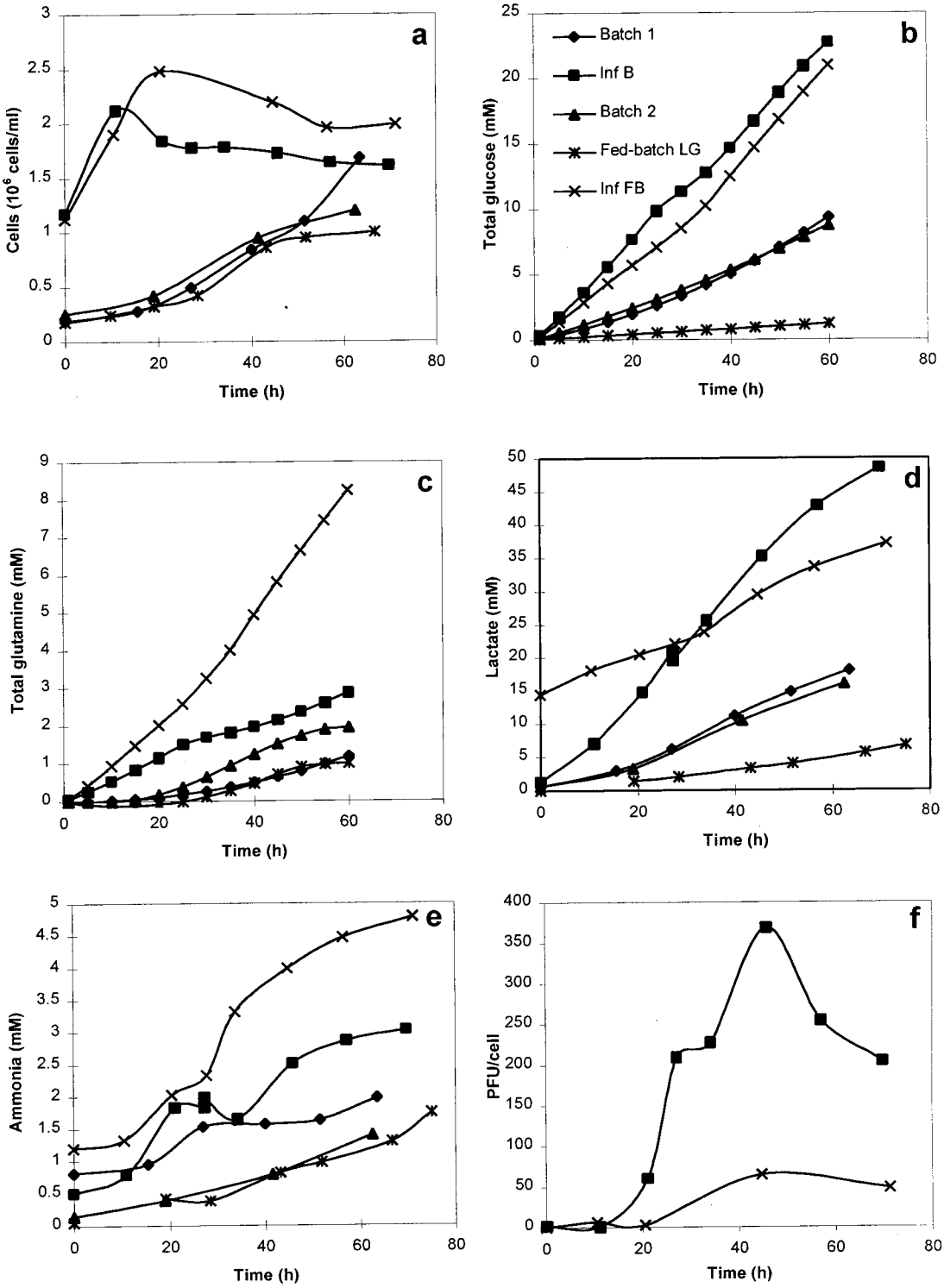

Figure 5. Cell growth (a), total glucose consumption (b), total glutamine consumption (c), lactate production (d), ammonia production (e), and virus titer (f) during growth and infection for each experiment.

ylalanine, tyrosine, valine or methionine are not increased, leading to an unbalanced Krebs cycle. All or part of the above events may explain the earlier plateau phase observed in batch 2.

The growth arrest in Batch 2 was not due to any observable limitations. The differences between the two batches may be attributed only to the high glutamine consumption and ammonia production compared to Batch 1. Noteworthy, Batch 1 had already some ammonia present in the medium; therefore, the cell had to regulate its glutamine consumption and ammonia production earlier in culture process.

Negative fluxes that were observed for F28 and F29 during exponential growth need to be discussed. The associated reactions are irreversible, so negative fluxes mean that the consumption rate did not meet the requirement for protein synthesis that was assumed in the model. This implies that either the cell metabolism was too low to meet this requirement or that there was an overestimation of protein synthesis mainly due to the measurement method for total proteins (see Materials and Methods).

Fed-Batch with Low Glucose. For the fed-batch with low glucose at 1 mM, there is clearly a plateau phase

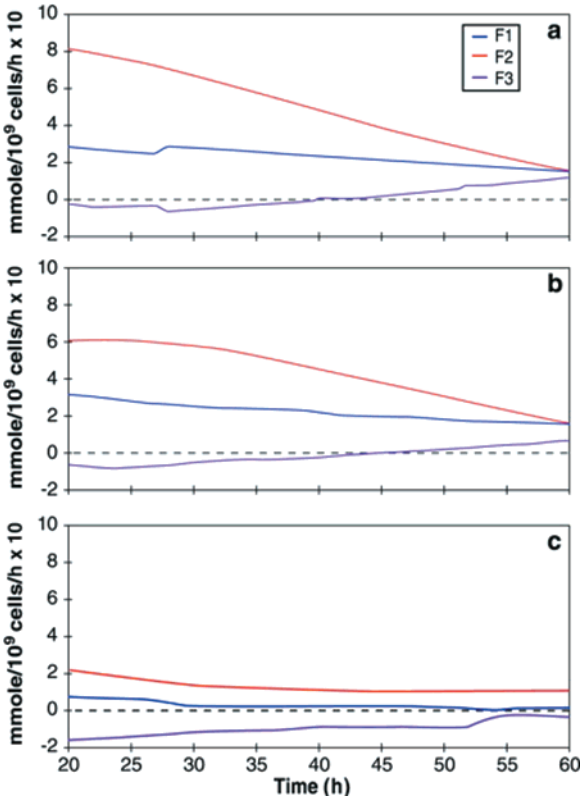

Figure 6. Glycolytic fluxes. Batch 1 (a), Batch 2 (b), Fed-Batch LG (c).

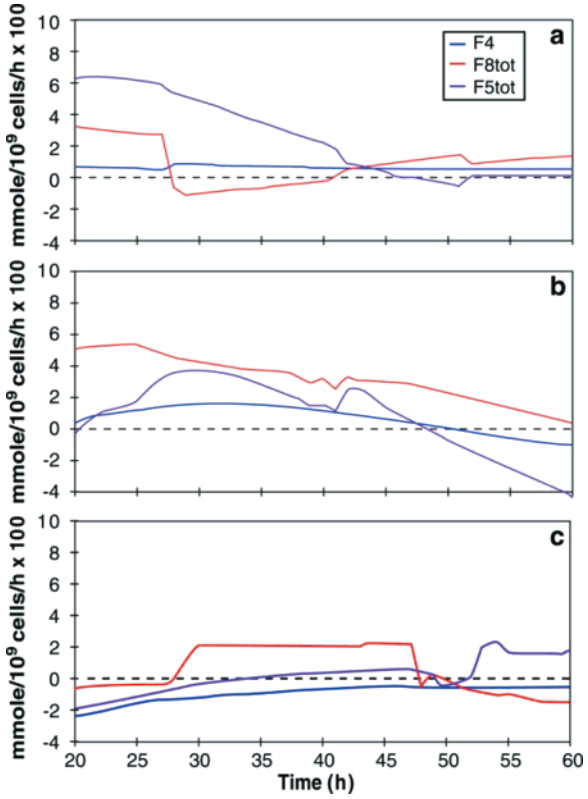

Figure 8. Glutaminolytic fluxes. Batch 1 (a), Batch 2 (b), Fed-Batch LG (c).

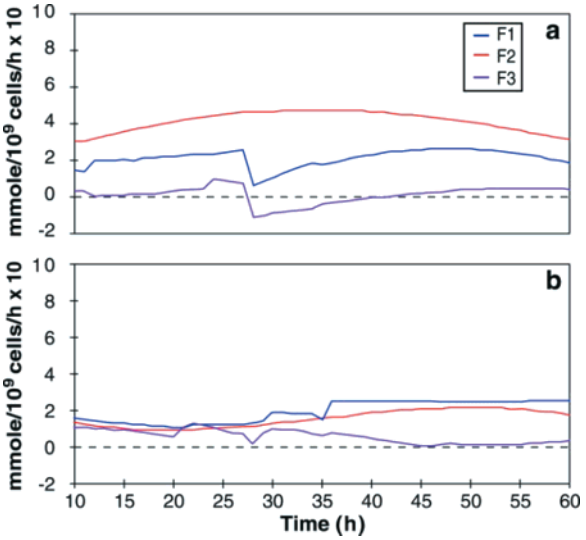

Figure 7. Glycolytic fluxes. Inf B (a), Inf FB (b).

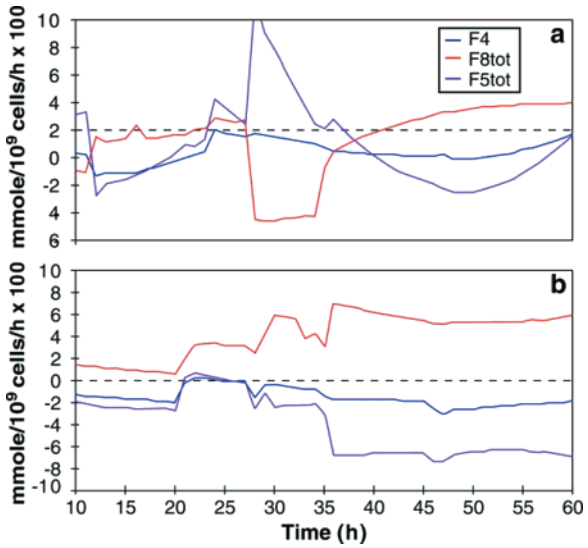

Figure 9. Glutaminolytic fluxes. Inf B (a), Inf FB (b).

observed at 45 h (Figure 5). Compared to the batches most of the glycolytic fluxes and glutaminolysis fluxes were lower while the amino acids and Krebs cycle fluxes were higher. Also, the net alanine flux (F4) is reversed. As previously reported, when glutamine or glucose consumption is reduced mammalian cells tend to use more amino acids (Cruz et al., 1999; Nadeau et al., 2000). It is interesting to note that during growth phase, F10 (the anaplerotic pathway) was very negative, meaning that most of the pyruvate enters the Krebs cycle in this way. The cells use the glucose in a more efficient way, by directing pyruvate to the Krebs cycle instead of metabolizing it to lactate.

At around 45−50 h, a metabolic change occurred as all the fluxes decreased while the cell growth rate diminished (Figure 5). The only flux that stayed high was $F5_{tot}$, the flux of glutamate to the Krebs cycle. This also corresponded to the point where glutamine consumption decreased (Figure 5) even though its concentration was still at 4 mM. Since ammonia concentration was at 1 mM and continued to be produced (Figure 5), ammonia accumulation might not be responsible for the metabolic change. As a matter of fact, some nonessential amino acids, aspartate, glutamate, and serine, became limiting at 50−60 h, although glutamate was produced shortly afterward (results not shown). These limitations could explain the metabolic changes. Siegwart et al. (1999) reported in the same manner that most of the specific consumption and production parameters dropped at 1×10^6 cells/mL during fed-batch with low glucose, except

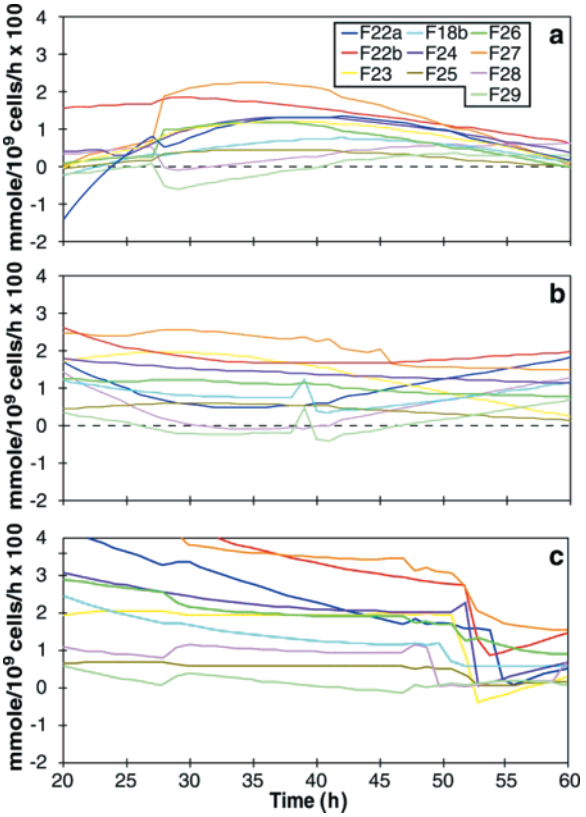

Figure 10. Amino acid fluxes. Batch 1 (a), Batch 2 (b), Fed-Batch LG (c).

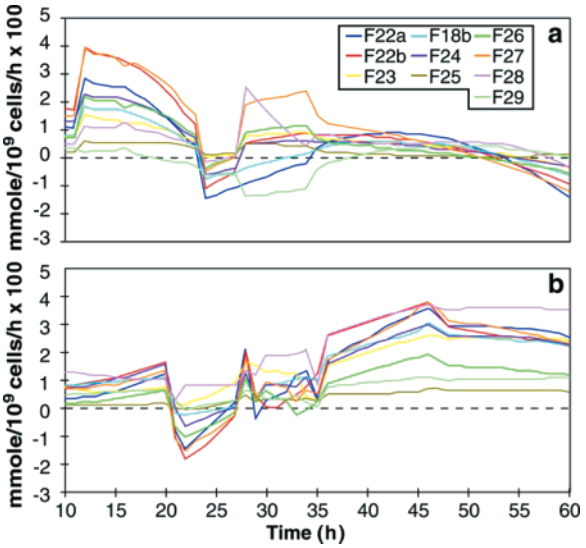

Figure 11. Amino acid fluxes. Inf B (a), Inf FB (b).

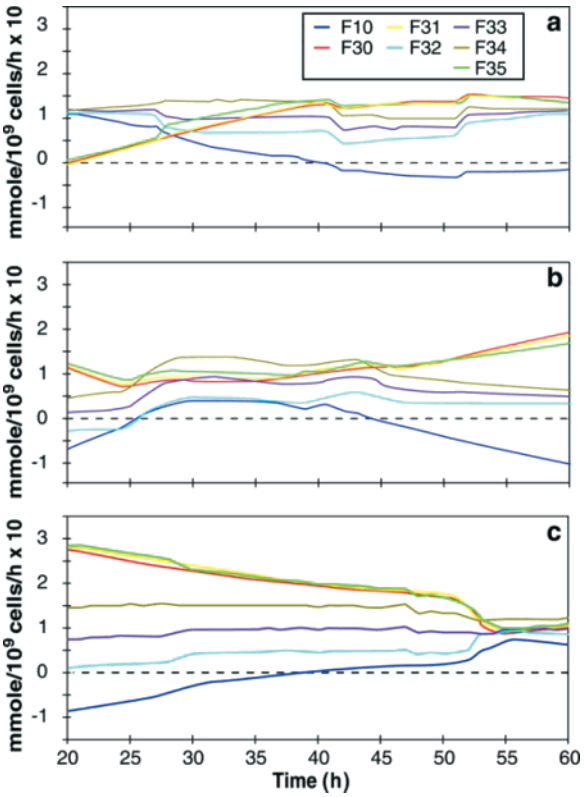

Figure 12. TCA cycle fluxes. Batch 1 (a), Batch 2 (b), Fed-Batch LG (c).

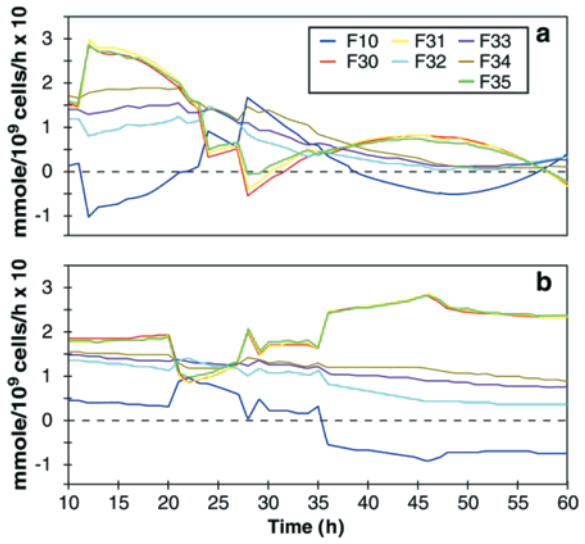

Figure 13. TCA cycle fluxes. Inf B (a), Inf FB (b).

for q_{O_2} and the growth rate. In fact, in the first growth part, the cells utilized nonessential amino acids as well as essential amino acids, but it seems that when the nonessential amino acids became limiting the cells shifted to a more efficient metabolism, reducing the amino acid fluxes as well as the Krebs cycle fluxes. However, this shift also led to a poorer growth rate.

Here again, we observed negative amino acids and Krebs cycle fluxes at certain times. These artifacts may be attributed to similar reasons as exposed in the preceding section.

Infection Phase. From Figure 5f we clearly see that the titer was much higher in the case of Inf B. This experiment had a normal infection process as can be shown by various parameters. First, we saw in Figure 2 an increase in the dry weight and total protein for Inf B. We know that this increase was due to accumulation of viral proteins, as the maximum in virus titer was also obtained at this time. After the peak was attained, it seems that proteins were degraded as the total protein decreased. A decrease was also observed with the viral titer. However, DNA synthesis in Inf B is still active after the peak in viral titer. Similarly, Wigand and Kumel (1978) saw a maximum in DNA production at around 20 h postinfection, which then dropped drastically. Usually DNA is stable and a drop in content may indicate that the cell integrity is affected. Therefore, for Inf B, it is not clear whether the loss in titer was due to an intracellular process that affected the virion as well as

the total proteins, but not DNA, or if the cell integrity was affected as the viability started to decrease and proteins were released in the extracellular medium (results not shown), or a combination of both phenomenons.

For Inf B, the growth stopped very early. Furthermore, we saw that at 10 h, there was an increase of most fluxes. This point corresponds to the onset of virion production, which clearly begins at 10 h after infection. The glycolytic fluxes increased during the infection phase reaching a maximum at 33 h. This observation has been reported before for 293S cells (Nadeau et al., 1996). Although the glycolytic and glutaminolytic fluxes remained similar to those in the growth phase, the amino acids fluxes and Krebs cycle fluxes are globally higher at the beginning of the infection. All of these events were not observed in Inf FB. In both infection experiments, F3 was slightly higher, showing that pyruvate was processed to acetyl-CoA, which entered the Krebs cycle through F35. F10 was also very negative at some points showing the entrance of pyruvate through the anaplerotic pathway. From all these observations, it seemed that the cell became more oxidative and used additional carbon sources other than glucose at the beginning of infection.

In addition, for both infection experiments at around 20 h, a decrease in the amino acid fluxes is observed. At around 27 h, a peak is observed for most of the amino acid fluxes. Although the peak observed in Inf B may be caused by two phenomena, infection and pulse addition. It was demonstrated that the fluxes were directly correlated to their corresponding nutrient concentrations in the medium (results not shown), showing that higher nutrient feeding and concentration stimulates the metabolism. However, the peak observed in Inf FB was not due to pulse feeding. From the observation of metabolic fluxes profile, it may have been more suitable to feed the cells earlier in order to counteract the negative amino acids fluxes observed at 20 h. As high amino acid fluxes were observed, we also saw a high glutamate flux ($F5_{tot}$), accompanied by a decreased glutamine flux ($F8_{tot}$), and at the same time the cells produced less ammonia. Even though glutamine was fed, its flux did not increase. However, tyrosine and phenylalanine fluxes (F26 and F27) became higher, providing glutamate but no ammonia. The cells preferred amino acids to glutamine as an energetic source during infection. On the contrary, the ammonia production was very high for Inf FB. It slowed around 20 h as in Inf B, but the production restarted afterward. The cells did not regulate its production tightly as in Inf B, and $F8_{tot}$, the glutamine consumption, remained very high.

Another interesting point was that the highest amino acid flux is the arginine flux for both infection processes. This is normal if we consider that the feedings were done with MEM amino acids in which the highest amino acid concentration is arginine. Noteworthy, arginine had been demonstrated as absolutely necessary for adenovirus production (Bonifas, 1967; Clark Rouse and Schlesinger, 1967; Heilman and Rouse, 1980; Kumel and Hammer, 1979; Wigand and Kumel, 1978). Clark Rouse and Schlesinger, (1967) had proposed earlier that arginine played a specific role in a late synthetic step for virion maturation. Without arginine, there was no virion production, but if arginine was added at 28−32 h after infection, the virion production was restored. As a matter of fact, in Inf B, a peak is observed at around 29 h, which is 15 h before the peak for adenovirus production.

As mentioned earlier, Inf B had a normal maximum titer compared to Inf FB. Regardless of the infection process (batch with medium renewal vs fed-batch without medium removal), this could also be due to the state of the cells before infection. Inf B was done with Batch 1, while Inf FB was done with Batch 2. As observed previously the Krebs cycle fluxes for Batch 2 were no more in steady state at infection time.

Furthermore, if we investigate for limitations during the infections (results not shown), in Inf FB aspartate was always null, serine dropped to zero at 20 h, and glycine at 35 h, while glutamate was produced afterward. In Inf B, glutamate and aspartate dropped to zero at 20 h, but glutamate was produced shortly afterward. Serine became limiting at 35 h. So limitations are observed earlier in the process for Inf FB, probably as a result of the higher cell concentration in bioreactor combined to an insufficient fed-batch rate and no medium renewal.

The observations for Inf FB indicate that the cells may not have been entirely infected by adenovirus, which is shown by the high growth and increased fluxes during infection, or, to a lesser extent, that the fed-batch rate in spent medium was not enough to sustain the infection and expression at such a cell concentration.

Conclusion.

The flux analysis permitted the extraction of more information from the data and allowed better understanding of the metabolism. Although all the singularities could not and should not be explained because of the sensitivity of the method, some relevant trends could be underlined, and comparisons from run to run could point out the role of key nutrients:

- Ammonia seemed to be a major regulator, as the cells produced no more than a certain amount during growth (1.5 mM). Therefore, the metabolism was adapted in order to meet this condition, shifting to the degradation of less ammoniagenic amino acids such as tyrosine and phenylalanine.
- Deviation from steady state in Krebs cycle fluxes may explain the earlier plateau phase for Batch 2.
- Although the glycolytic and glutaminolytic fluxes were lower for the fed-batch with low glucose, the amino acids fluxes, as well as the Krebs cycle fluxes, were higher at the beginning of the run.

Metabolic flux analysis was also used to study the infection phase and some trends could be pointed out during a normal infection process:

- increase in dry weight, total protein, and DNA content
- increase in glycolytic fluxes up to a maximum
- more pyruvate entering the Krebs cycle via acetyl-CoA and the anaplerotic pathway (F3 and F10)
- increase in amino acids fluxes at 10 h and near 30 h
- preference for amino acid instead of glutamine
- from these observation it is clear that Inf FB was not optimized as we could observe some but not all of the above indicators.

Metabolic flux patterns are then useful to evaluate the culture state during growth and infection and will further help to develop feeding strategies:

- stability evaluation of the Krebs cycle fluxes before infection
- earlier pulse addition during the batch process for infection to prevent negative fluxes
- higher fed-batch rates to prevent negative fluxes but also limitations in nonessential amino acids

References and Notes

Babich, A.; Feldman, L. T.; Nevins, J. R.; Darnell, J. E.; Weinberger, C. Effect of Adenovirus on Metabolism of Specific

Host mRNAs: Transport Control and Specific Translational Discrimination. *Mol. Cell, Biol.* **1983**, *3*, 1212−1221.
Bannai, S. Exchange of Cystine and Glutamate across Plasma Membrane of Human Fibroblasts. *J. Biol. Chem.* **1986**, *261*, 2256−2263.
Bannai, S.; Ishii, T. A Novel Function of Glutamine in Cell Culture: Utilization of Glutamine for the Uptake of Cystine in Human Fibroblasts. *J. Cell. Physiol.* **1988**, *137*, 360−366.
Bonarius, H. P. J.; Hatzimanikatis, V.; Meesters, K. P. H.; de Gooijer, C. D.; Georg, S.; Tramper, J. Metabolic Flux Analysis of Hybridoma Cells in Different Culture Media Using Mass Balance. *Biotechnol. Bioeng.* **1996**, *50*, 299−318.
Bonarius, H. P. J.; Schmid, G.; Tramper, J. Flux Analysis of Underdetermined Metabolic Networks: The Quest for the Missing Constraints. *Trends Biotechnol.* **1997**, *15*, 307−315.
Bonifas, V. H. Time-Course and specificity of the Arginine Requirement for Adenovirus Biosynthesis. *Arch. Gesamte Virusforsch.* **1967**, *20*, 20−28.
Boucher, R. C.; Knowles, M. R. Gene Therapy for Cystic Fibrosis Using E1-Deleted Adenovirus: a Phase 1 Trial in the Nasal Cavity. *Hum. Gene Ther.* **1994**, *5*, 615−634.
Briand, P.; Kahn, A. Interets et limites des vecteurs adenoviraux pour le transfert de genes in vivo. *Pathol. Biol.* **1993**, *41*, 663−671.
Brown, R. R. Metabolism and Biology of Tryptophan. In *Recent Advances in Tryptophan Research*; Fillipini, G. A., Costa, C. V. K., Bertazzo, A., Eds.; Plenum Press: New York, 1996; pp 15−25.
Clark Rouse, H.; Schlesinger, R. W. An Arginine-Dependent Step in the Maturation of Type 2 Adenovirus. *Virology* **1967**, *33*, 513−522.
Côté, J.; Garnier, A.; Massie, B.; Kamen, A. Serum-Free Production of Recombinant Proteins and Adenoviral Vectors by 293SF-3F6 Cells. *Biotechnol. Bioeng.* **1998**, *59*, 567−575.
Cruz, H. J.; Moreira J. L.; Carrondo, M. J. T. Metabolic Shifts by Nutrient Manipulation in Continuous Cultures of BHK Cells. *Biotechnol. Bioeng.* **1999**, *66*, 104−113.
Crystal, R. G.; Mcelvaney, N. G.; Rosenfeld, M. A.; Chu, C. S.; Mastrangeli, A.; Hay, J. G.; Brody, S. L.; Jaffe, H. A.; Eissa, N. T.; Danel, C. Administration of an Adenovirus Containing the Human CFTR cDNA to the Respiratory Tract of Individuals with Cystic Fibrosis. *Nat. Genet.* **1994**, *8*, 42−51.
Garnier, A.; Coté, J.; Nadeau, I.; Kamen, A.; Massie, B. Scale-Up of the Adenovirus Expression System for the Production of Recombinant Protein in Human 293S Cells. *Cytotechnology* **1994**, *15*, 145−155.
Graham, F. L.; Smiley, J.; Russel, W. C.; Nairn, R. Characteristics of a Human Cell Line Transformed by DNA from Human Adenovirus Type 5. *J. Gen. Virol.* **1977**, *36*, 59−74.
Gray, D. R.; Chen, S.; Howarth, W.; Inlow, D.; Maiorella, B. L. CO_2 in Large-Scale and High-Density CHO Cell Perfusion Culture. *Cytotechnology* **1996**, *22*, 65−78.
Green, M. Biochemical Studies on Adenovirus Multiplication. Xll. Plaquing Efficiencies of Purified Human Adenovirus. *Virology* **1967**, *31*, 562−565.
Green, M. Effect of Oncogenic DNA Viruses on Regulatory Mechanisms of Cells. *Fed. Proc.* **1970**, *29*, 1265−1275.
Heilman, C. A.; Rouse, H. Adenovirus Type 2 Polypeptide Synthesis in Arginine-Deprived Cells. *Virology* **1980**, *105*, 159−170.
Hodge, L. D.; Scharff, M. D. Effect of Adenovirus on Host Cell DNA Synthesis in Synchronized Cells. *Virology* **1969**, *37*, 554−564.
Kamen, A.; Tom, R.; Caron, A.; Chavarie, C.; Massie, B.; Archambault, J. Culture of Insect Cells in a Helical Ribbon Impeller Bioreactor. *Biotechnol. Bioeng.* **1991**, *38*, 619−628.
Kay, M. A.; Woo, S. L. C. Gene Therapy for Metabolic Disorders. *Trends Genet.* **1994**, *10*, 253−257.
Kooistra, T.; Lloyd, J. B. Degradation of Insulin by Human Fibroblasts: Effects of Inhibitors of Pinocytosis and Lysosomal Activity. *Int. J. Biochem.* **1985**, *17*, 805−811.
Kooistra, T.; Lloyd, J. B. Pinocytosis and Degradation of Exogenous Proteins by Cystinotic Fibroblasts. *Biochim. Biophys. Acta* **1986**, *887*, 182−186.
Kumel, G.; Hammer, H. J. The Influence of Arginine Starvation on the Synthesis of Virus High Molecular Weight DNA in Hela Cells Productively Infected by Adenovirus Type 5. *J. Gen. Virol.* **1979**, *45*, 599−610.
Lindberg, U.; Persson, T.; Philipson, L. Isolation and Characterization of Adenovirus Messenger Ribonucleic Acid in Productive Infection. *J. Virol.* **1972**, *10*, 909−919.
Mancuso, A.; Sharfstein, S. T.; Tucker, S. N.; Clark, D. S.; Blanch, H. W. Examination of Primary Metabolic Pathways in a Murine Hybridoma with Carbon-13 Nuclear Magnetic Resonance Spectroscopy. *Biotechnol. Bioeng.* **1994**, *44*, 563−585.
Nadeau, I.; Garnier, A.; Côté, J.; Massie, B.; Chavarie, C.; Kamen, A. Improvement of Recombinant Protein Production with the Human Adenovirus/293S Expression System Using Fed-Batch Strategies. *Biotechnol. Bioeng.* **1996**, *51*, 613−623.
Nadeau, I.; Sabatié, J.; Koehl, M.; Perrier, M.; Kamen, A. Human 293 Cell Metabolism in low Glutamine-Supplied Culture: Interpretation of Metabolic Changes through Metabolic Flux Analysis. *Metab. Eng.* **2000**, in press.
Nyberg, G. B.; Balcarcel, R. R.; Follstad, B. D.; Stephanopoulos, G.; Wang, D. I. C. Metabolism of Peptide Amino Acids by Chinese Hamster Ovary Cells Grown in a Complex Medium. *Biotechnol. Bioeng.* **1999**, *62*, 324−335.
Petch, D.; Butler, M. Profile of Energy metabolism in a Murine Hybridoma: Glucose ad Glutamine Utilization. *J. Cell. Physiol.* **1994**, *161*, 71−76.
Philipson, L.; Pettersson, U.; Lindberg, U.; Tibbetts, C.; Vennstrom, B.; Persson, T. RNA Synthesis and Processing in adenovirus infected cells. *Cold Spring Harbor Symp. Quant. Biol.* **1975**, *39*, 447−456.
Pina, M.; Green, M. Biochemical Studies on Adenovirus Multiplication. XLV. Macromolecule and Enzyme Synthesis in Cells Replicating Oncogenic and Nononcogenic Human Adenovirus. *Virology* **1969**, *38*, 573−586.
Pissarra, P. d. N.; Henriksen, C. M. Fluxmap. A Visual Environment for Metabolic Flux Analysis of Biochemical Pathways. In *Computer Applications in Biotechnology*; Yoshida, T., Shioya, S., Eds.; Osaka, Japan, 1998.
Salway, J. G. *Metabolism at a Glance*, 1st ed.; Blackwell Scientific Publications: Oxford, 1994.
Savinell, J. M.; Palsson, B. O. Optimal Selection of Metabolic Fluxes for in vivo Measurements. 1. Development of Mathematical Methods. *J. Theor. Biol.* **1992**, *155*, 201−214.
Schmid, G.; Keller, T. Monitoring Hybridoma Metabolism in Continuous Suspension Culture at the Intracellular Level. *Cytotechnology* **1992**, *9*, 217−229.
Schmidt, K.; Marx, A.; de Graaf, A. A.; Wiecher, W.; Sahm, H.; Nielson, J.; Villadsen, J. 13C Tracer Experiments and Metabolite Balancing for Metabolic Flux Analysis: Comparing Two Approaches. *Biotechnol. Bioeng.* **1998**, *58*, 254−257.
Siegwart, P.; Male, K.; Côté, J.; Luong, J. H. T.; Perrier, M.; Kamen, A. Adaptative Control at Low-Level Glucose Concentration To Study HEK-293 Cell Metabolism in Serum Free Cultures *Biotechnol. Prog.* **1999**, *15*, 608−616.
Takiguchi, N.; Shimizu, H.; Shioya, S. An On-Line Physiological State Recognition System for the Lysine Fermentation Process Based On a Metabolic Reaction Model. *Biotechnol. Bioeng.* **1997**, *55*, 170−181.
Trapnell, B. C. Adenoviral Vectors for Gene Transfer. *Adv. Drug Delivery Rev.* **1993**, *12*, 185−199.
Trapnell, B. C.; Gorziglia, M. Gene Therapy Using Adenoviral Vectors. *Curr. Opin. Biotechnol.* **1994**, *5*, 617−625.
White, D. O.; Scharf, M. D.; Maizel, J. V. The Polypeptides of Adenovirus lll. Synthesis in Infected Cells. *Virology* **1969**, *3*, 395−406.
Wigand, R.; Kumel, G. Amino Acid Requirement of Adenovirus Multiplication. *J. Gen. Virol.* **1978**, *39*, 281−292.
Xie, L.; Wang, D. I. C. Applications of Improved Stoichiometric Model in Medium Design and Fed-Batch Cultivation of Animal Cells in Bioreactor. *Cytotechnology* **1994**, *15*, 17−29.
Xie, L. Z.; Wang, D. I. C. Stoichiometric Analysis of Animal Cell Growth and Its Application in Medium Design. *Biotechnol. Bioeng.* **1994**, *43*, 1164−1174.

Accepted for publication August 7, 2000.

BP000098L